




Composite phospholipid-coated hollow mesoporous silica nanoplatfom with multi-stimuli responsiveness for combined chemo-photothermal therapy

Yifan Wu¹, Junya Lu¹, Yuling Mao¹, Tongying Jiang¹, Qinfu Zhao^{1,*}, and Siling Wang^{1,*} 

¹Department of Pharmaceutics, School of Pharmacy, Shenyang Pharmaceutical University, 103 Wenhua Road, Shenyang 110016, Liaoning Province, People's Republic of China

Received: 30 October 2019

Accepted: 16 December 2019

Published online:
21 January 2020

© Springer Science+Business Media, LLC, part of Springer Nature 2020

ABSTRACT

Chemo-photothermal therapy can improve the therapeutic effects of simple chemotherapy with the help of cytotoxic heat generated by photothermal therapy. In this paper, a novel nanoplatfom based on hollow mesoporous silica (HMSN) was constructed, which could achieve multi-stimuli-responsive release through chemo-photothermal interaction. Cypate as a NIR photothermal agent was conjugated to the outer surface of HMSN by disulfide bonds. Due to the insoluble feature, Cypate imparted lipophilicity to the surface of HMSN, thereby promoting the strong encapsulation of complex phospholipid layer by hydrophobic interaction. The phospholipid layer hindered the premature release of the model drug doxorubicin (DOX), prolonged the circulation time in vivo, and improved the biocompatibility and stability in physiological environment. Under glutathione, acidic conditions and NIR irradiation, the release of DOX was significantly accelerated, indicating that DOX/HMSN-CyL exhibited redox/pH/NIR multi-stimuli in response to drug release. Cytotoxicity experiments have proved that combination therapy induced the maximum levels of cell killing. Furthermore, combination index of DOX/HMSN-CyL was 0.26, demonstrating the chemo-photothermal synergetic therapy. Multicellular tumor spheroid experiments were also performed, and the same trend was showed. In summary, this novel nanoplatfom has broad application prospects as a drug delivery system for combination therapy.

Introduction

At the present time, cancer has become one of the major health threats worldwide. Radiation therapy and surgery are only suitable for early patients, so

chemotherapy is still the most important means of treating malignant tumors in the middle and late stages. Traditional chemotherapeutic drugs are non-specifically distributed in tumor sites which could

Address correspondence to E-mail: qinfuzhao@syphu.edu.cn; silingwang@syphu.edu.cn

produce non-selective toxicity to normal tissue cells and tumor cells, causing serious side effects. Therefore, stimuli-responsive drug delivery systems (SDDS) have been designed to solve the above problems. SDDS allow drugs to be released in response to internal or external stimuli such as pH [1–3], redox potential [4–7], enzyme [8, 9], light [10–12], or temperature changes [13, 14], aiming to improve the treatment effect and reduce side effects. In addition, another impediment of chemotherapy is multidrug resistant (MDR) caused by a variety of mechanisms, such as accelerating the efflux of anticancer drugs interceded by P glycoprotein membrane transporters [15–18]. Thus, it is very vital and necessary to develop synergistic antitumor treatments. Among these new therapies, the combination of photothermal therapy (PTT) and chemotherapy has made significant progress in synergistic cancer treatment. Since cancer cells are more sensitive to heat than normal cells, cytotoxic heat can destroy the membrane structure and organelles of cells and interfere with their normal metabolism, thus leading to cell apoptosis. Hyperthermia can also induce tumor-specific cellular uptake and trigger the release of drugs from nanoparticles, thereby exerting synergy with chemotherapy [19]. Effective heat can increase the sensitivity of tumor cells and reverse multidrug resistance [20, 21], so the drug dosage requirements can be reduced to lessen the side effects of chemotherapy.

Near-infrared light (NIR, $\lambda = 700\text{--}1100\text{ nm}$) is widely used in PTT research because of its high selectivity, small damage to human body, and strong tissue penetration [22]. There are many types of NIR photothermal conversion agents, such as gold nanorods based on precious metals [23], graphene based on carbon elements [24], and carbocyanine dyes based on organics [25]. These photothermal conversion agents play a key role in PTT. Among these materials, the organic substance Cypate was selected for PTT, and the reasons are as follows: (1) Cypate is a NIR-absorbing cyanine dye with low radiation transition and a large molar extinction coefficient, which has good photothermal conversion efficiency [26]. (2) Cypate is lipophilic and can be used as a “gate” to prevent the early release of drugs [27]. (3) Cypate is an analog of ICG (FDA approved medical imaging probe) that demonstrates its safety [28]. However, ICG is not easy to modify, and Cypate has a carboxyl group at each end of the chain that can

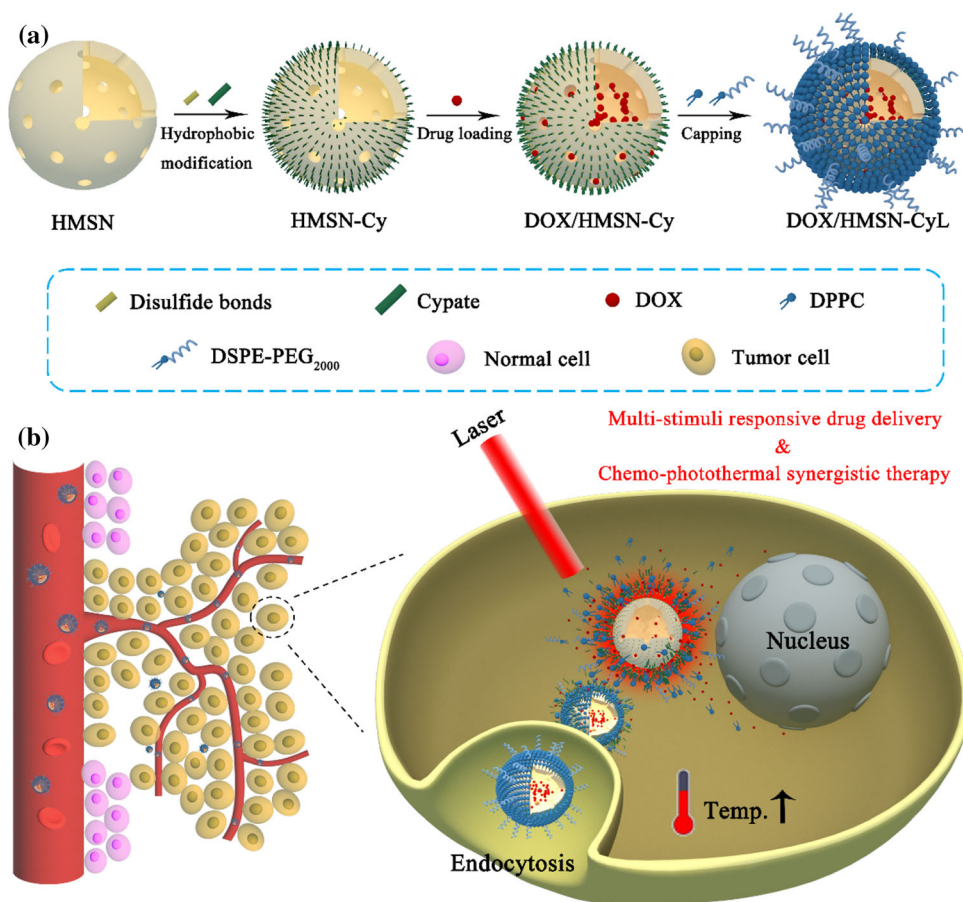
be functionally modified, which is advantageous for the construction of nanoformulations. In view of these advantages, Cypate was selected as a NIR photothermal conversion agent in our work.

Hollow mesoporous silica (HMSN) was selected as the drug carrier because of its large surface area, pore volume, and easy-to-modify surfaces, which could be used to connect “doors and switches” to subtly control drug release. Compared with mesoporous silica nanoparticles, HMSN with the hollow structure is favorable for high drug loading. Further, it is known that the skeleton of silica can be excreted from the feces or urine substantially in the form of hepatobiliary circulation and renal secretion after four weeks of administration, and thus, it is considered to be safe [29, 30]. Unlike other design systems that incorporate Cypate into nanoparticles, Cypate is innovatively grafted onto the surface of HMSN via disulfide bonds as a NIR light absorber to generate photothermal (HMSN-Cy). Since the concentration of intracellular glutathione (GSH) in most cancer cells is almost 100–1000 times higher than in the extracellular environment, GSH may be a stimulator of SDDS. This means that the hydrophobic Cypate layer bonded to the surface of HMSN can be stabilized in the extracellular environment during the cycle and shed in tumor cells under high concentration of GSH.

To obtain a nanoparticle with a hydrophilic surface, the complex phospholipid containing 1,2-dipalmitoyl-*sn*-glycero-3-phosphatidylcholine (DPPC) and 1,2-distearoyl-*sn*-glycero-3-phosphoethanolamine-*N*-[amino(poly(ethylene glycol))-2000] (DSPE-PEG₂₀₀₀) was further coated on the surface of HMSN-Cy. The complex phospholipid coating can avoid the aggregation and hemolysis characteristics of HMSN under physiological environment, prolong the blood retention time, prevent nanoparticles from being taken up by non-specific macrophages, and prolong the circulation time after intravenous injection (PEG chain in DSPE-PEG₂₀₀₀). The composite phospholipid layer not only improves the stability of the nanoparticles, but also acts as a “gate” to prevent pre-leakage of the drug. However, it is well known that the study of lipid layer and Cypate-coated HMSN as a photothermal agent for PTT has not been reported.

In this work, a multi-response delivery system with good heat efficiency and good dispersion was designed (Scheme 1). The near-infrared-absorbing agent Cypate was coated on the surface of HMSN (HMSN-Cy) by disulfide bonds to prevent premature

Scheme 1 a Synthesis route of DOX/HMSN-CyL. b Combined photothermal therapy and chemotherapy for tumors.



release of doxorubicin (DOX) and imparted photothermal properties to the system. Then, the composite phospholipid molecular layer was further coated on the surface of HMSN-Cy by hydrophobic force (HMSN-CyL) to extend the cycle time and improve the biocompatibility and dispersion stability of nanoparticles in physiological environment. Based on previous reports, since the release profile of DOX from HMSN carrier was pH responsive, this could realize stable drug delivery under normal physiological conditions, as well as on-demand release behavior in an acidic tumor microenvironment. DOX/HMSN-CyL had a good heating effect under NIR radiation and exhibited the characteristics of redox/pH/NIR multi-stimuli triggered drug release. The high temperature generated by PTT could further promote the release of DOX, thereby producing a synergistic effect on tumor cells. In summary, a multi-stimuli-responsive system was simply constructed by hydrophobic interaction, and an effective drug loading was achieved, which made the drug

loading system have broad application prospects in combination therapy.

Materials and methods

Materials and chemical reagents

Tetraethoxysilane (TEOS), cetyltrimethylammonium bromide (CTAB), 3-mercaptopropyltrimethoxy silane (MPTMS, 95%), GSH, *N*-(3-dimethylaminopropyl)-*N*-ethyl carbodiimide hydrochloride (EDC), *N*-hydroxy succinimide (NHS), fetal bovine serum (FBS), Roswell Park Memorial Institute (RPMI)-1640 and fluorescent Hoechst 33258, propidium iodide (PI), calcein-AM, doxorubicin hydrochloride (DOX) were acquired from Dalian Meilun Biotech Co., Ltd (Dalian, China). The DSPE-PEG₂₀₀₀ and DPPC were all offered by A.V.T. (Shanghai, China). 3-(4,5-Dimethylthiazol-2-yl)-2,5-diphenyl tetrazolium bromide (MTT) was obtained from Amresco (USA). NIR fluorescence dye Cypate was synthesized according to previous method [31]. All other chemicals were

analytical grade and used without further purification.

Preparation of nanoparticles

Synthesis of HMSN-SH

The published literature had investigated the preparation of HMSN nanoparticles [32]. According to the reported literature, the thiol-functionalized HMSN (HMSN-SH) was prepared by post-grafting method [33]. The ratio of MPTMS to HMSN was 1:4 (m/v). Then, the product was refluxed in ethanol containing NH_4NO_3 (1.5 g) for 9 h to obtain CTAB-free carriers.

Synthesis of HMSN-SS-NH₂

The synthesis of S-(2-aminoethylthio)-2-thiopyridine hydrochloride (Py-SS-NH₂) has been previously studied [34]. Thereafter, 50 mg of Py-SS-NH₂ was added to 30 mL of ethanol containing 250 mg of HMSN-SH and then stirred at 25 °C for one day, and finally, the nanoparticles were collected by centrifugation.

Synthesis of HMSN-Cy

First, 50 mg of Cypate was added to DMSO and sonicated, and then, EDC and NHS were added to activate at 30 °C for 1 h, and finally, the carrier HMSN-SS-NH₂ was added. The entire reaction should be stirred continuously for more than 24 h (30 °C), collected, and dried eventually.

Development of HMSN-CyL and drug loading

HMSN-CyL was prepared according to a modified thin-film hydration method. The hydrophobic HMSN-Cy was first put in 2 mL chloroform, sonicated to fully disperse, and then, the previously dissolved DPPC and DSPE-PEG₂₀₀₀ chloroform solution was added to the suspension. After sonicating to homogenize, the solution was evaporated to a uniform film under reduced pressure and was resuspended by ultrasound in pH 7.4 phosphate-buffered saline (PBS). HMSN-CyL can be obtained by centrifuging multiple times until excess DPPC and DSPE-PEG₂₀₀₀ are removed.

The drug was loaded before coating the composite phospholipid layer, and HMSN-Cy (10 mg) was incubated with 5 mL of DOX (2 mg/mL) in methanol for one day with constant stirring to allow the carrier to fully absorb the drug. After centrifugation, DOX-containing HMSN-Cy (DOX/HMSN-Cy) was obtained. The capping was conducted following the procedure described above. The amount of DOX loaded can be determined by subtracting the drug in the supernatant after drug loading from the total mass of the initially added drug.

Characterization of the nanoparticles

Transmission electron microscopy (TEM, Tecnai G2F30; FEI; Eindhoven, Netherlands) at 200 kV was used to observe the internal morphological characteristics. The crystalline structure was measured by X-ray diffraction (XRD, Rigaku Geigerflex X-ray diffractometer, Japan) with Cu-K α radiation ($\lambda = 1.5405 \text{ \AA}$) and differential scanning calorimeter (DSC, Mettler-Toledo, Switzerland). Particle size distributions and zeta potentials were detected by a Particle Size Analyzer Nicomp 380 (Particle Sizing Systems, USA). The surface area and pore size distribution were determined from N₂ adsorption/desorption isotherms collected by V-Sorb 2800P (Gold APP Instrument Corporation, Beijing, China). The optical properties were investigated by Fourier transfer infrared (FT-IR) spectra on Bruker IFS (Switzerland). Thermogravimetric analysis (TGA) was carried out using a TGA-50 instrument (Shimadzu, Japan) to study the weight loss after each step of functionalization at a heating rate of 10 °C/min under nitrogen. The Vis-NIR absorption spectra were recorded using a spectrophotometer (UV-4802, UNICO, Shanghai).

In vitro stimuli-responsive drug release

Drug release experiment was conducted as follows. 3 mg of DOX/HMSN-CyL samples was separately dispersed in pH 7.4 PBS (with or without 10 mM GSH), pH 5.0 PBS (with or without 10 mM GSH), and shaken at 100 rpm (37 °C). DOX concentration was measured and retracted at predetermined intervals. The released DOX was eventually monitored at 480 nm. The irradiation group was somewhat different from the other groups. It was exposed to NIR laser (808 nm, 1.5 W/cm²) for 2 min at 3 h, 6 h, and

9 h, respectively, and everything else was the same as above.

Dispersion stability and photothermal heating efficiency

Samples were separately dispersed in distilled water and pH 7.4 PBS (2 mg/mL). The stability and dispersibility of the samples (HMSN-CyL) were evaluated by measuring the particle size and polydispersity index (PDI) at the designated time points.

HMSN-CyL was dispersed in different volumes of distilled water and adjusted to different concentrations; then, pipette 200 μL of the sample into a 0.5-mL EP tube. The samples were irradiated at a fixed power density (1.5 W/cm^2) at different concentrations and different power densities at a fixed concentration (500 $\mu\text{g}/\text{mL}$). Distilled water was irradiated as a negative control. Thermal imager recorded the heating data and then plotted the temperature rise curve. To calculate the photothermal conversion efficiency, HMSN-CyL suspension (500 $\mu\text{g}/\text{mL}$, 200 μL) was irradiated, followed by naturally cooling to room temperature without irradiation. Details of the calculation are given in the supporting information.

Cellular photothermal effects induced by NIR laser

4T1 cells were seeded in 6-well plates for 24 h (37 $^{\circ}\text{C}$, 5% CO_2) and then incubated with HMSN-CyL for 2 h. Thereafter, 4T1 cells were collected and the nanoparticles that were not uptake by the cells were removed, and finally, the temperature changes were monitored using a thermal imager with NIR laser irradiation (1.5 W/cm^2) for 3 min.

Hemolysis study and BSA absorption measurement

Hemolysis study and BSA absorption measurement experiments were carried out according to previous reports [35]. The mixed solution including samples and diluted red blood cell (RBC) suspension was allowed to stand, photographed, and centrifuged to remove the supernatant clear solution, which was measured at 541 nm using a UV-vis spectrophotometer. Hemolysis of RBC in saline and distilled

water was used as a negative and positive control, individually. As well, the BSA solution was stained with Coomassie Brilliant Blue, and the absorbance was measured at 595 nm using an UV-vis spectrophotometer for quantification.

Live/dead cell assay

The photothermal effects were further visualized by seeding 4T1 cells into 24-well plates. The medium was replaced with fresh medium containing 250 $\mu\text{g}/\text{mL}$ of HMSN-CyL and then irradiated with NIR laser for 5 min after 2-h incubation. Additionally, different concentrations of HMSN-CyL were added to a 24-well plate and irradiated with NIR laser at 2 W/cm^2 . After these, 4T1 cells were washed and stained with calcein-AM/PI according to product instructions and then observed by confocal laser scanning microscopy (CLSM, Zeiss LSM 510).

Cell uptake

Cell uptake of DOX/HMSN-CyL was assessed by CLSM and flow cytometry (FCM). 4T1 cells were treated with sterilized HMSN-CyL, DOX/HMSN-CyL, and free DOX (equal to 5 $\mu\text{g}/\text{mL}$ DOX). After continuing to incubate for 2 h, 4T1 cells were washed with PBS. For the NIR irradiation group, DOX/HMSN-CyL was irradiated with NIR laser (808 nm) and further incubated for 60 min. A well containing DOX/HMSN-CyL without NIR irradiation was used as a negative control after washing. After these, cells were stained with Hoechst 33258 and visualized in CLSM. The method of assessing cellular uptake of DOX/HMSN-CyL by FCM was similar to the above. After 2 h of incubation, FCM was used to measure DOX fluorescence.

In vitro cytotoxicity studies

For the cytotoxicity assay, 4T1 cells were cultured in a 96-well plate for one day, and then, the medium was replaced with gradient concentration nanocarrier solution and incubation was continued for one day. The NIR irradiation group was irradiated with 808 nm laser for 3 min (2.0 W/cm^2). Lastly, cell viability was measured using the MTT assay. Calculated combination index (CI): $\text{CI} = [\text{IC}_{50} (\text{combination therapy}) / \text{IC}_{50} (\text{chemotherapy only})] + [\text{IC}_{50} (\text{combination therapy}) / \text{IC}_{50} (\text{PTT alone})]$. A CI value

of < 1 indicates synergy, a CI value of > 1 indicates antagonism, and a CI value of 1 indicates an additive effect.

Therapeutic efficacy on multicellular tumor spheroids (MCTs)

The monolayer cultured 4T1 cells were trypsinized to prepare a single-cell suspension. The autoclaved 1% w/v agarose solution was applied to the bottom of a 96-well plate to form a depression. Cells were counted and seeded into 96-well plates approximately 3500 cells per well, and fresh medium was changed every two days. MCTs could be formed after 3–5 days and then incubated with different samples for 24 h. Finally, the size and morphology of the spheroid were studied using an inverted microscope equipped with a digital camera.

Results and discussion

Construction and characterization of HMSN-CyL

As described in Scheme 1, HMSN-CyL was prepared by grafting a hydrophobic dye Cypate on HMSN via disulfide bonds and using a lipid layer containing DPPC and DSPE-PEG₂₀₀₀ as a capping. First of all, the surface of HMSN was thiolated by MPTMS to obtain HMSN-SH, and then, HMSN-SS-NH₂ was obtained by disulfide exchange reaction. Finally, Cypate was covalently grafted onto the surface of HMSN by an amidation reaction, and the product was called HMSN-Cy. DPPC and DSPE-PEG₂₀₀₀ with a molar ratio of 4:1 were added to self-assemble into a composite phospholipid layer, acting as a cap for HMSN-Cy.

The prepared HMSN carrier showed a well-ordered mesoporous shell and a uniform hollow structure with an average diameter of 250 nm as shown in the TEM image (Fig. 1a). The shell had an average thickness of approximately 70 nm. Many other studies have reported that nanoparticles in the 50–300 nm range can guarantee an ideal EPR effect. Compared with the smooth surface of HMSN, the surface after coating with phospholipids was rough, indicating that DPPC and DSPE-PEG₂₀₀₀ were coated on the surface of HMSN (Fig. 1b).

To prove each step of grafting successfully, a series of experiments were essential. Zeta potential of HMSN-SH after NH₂ modification reversed from a negative value of -33 mV to a positive value of $+27$ mV (Tab. S1). After the phospholipid layer was coated on the surface of HMSN-Cy, the zeta potential was about $+2$ mV (Fig. 1c) due to the shielding effect of the neutrally charged lipid layer and PEG chain of DSPE. The successful connection of disulfide bonds was also confirmed by Raman spectroscopy (Fig. S1). The Raman extension occurring at 510 cm^{-1} compared to HMSN-SH was attributed to the formation of disulfide bonds. The above conclusion can also be obtained from the adsorption–desorption isotherm curve and pore size distribution measurement. HMSN-SH had a large specific surface area of $686.1\text{ m}^2/\text{g}$, which was supportive for achieving an elevated drug loading efficiency with an average pore diameter of 3.7 nm and total pore volume of $0.64\text{ cm}^3/\text{g}$ (Fig. 1d, e). After each grafting process, all three parameters of the HMSN materials were gradually reduced, especially the surface area dropped sharply to $21\text{ m}^2/\text{g}$ (Tab. S2). This indicated that the pores of the nanoparticles were completely blocked after being covered by the complex phospholipid layer. Thus, drug loading should be performed prior to the phospholipid layer capping process.

In Fig. 1I, the FT-IR spectra of HMSN nanoparticles are compared. The absorption peaks appeared at 1228 cm^{-1} and 1738 cm^{-1} belonged to P=O and C=O, representing the existence of a phospholipid layer on HMSN. Additionally, the grafting of phospholipid layer was confirmed by increased peaks around 2853 cm^{-1} and 2924 cm^{-1} , which were attributed to the vibration of CH₂ in the PEG of DSPE-PEG₂₀₀₀. This phenomenon is consistent in Fig. 1g. HMSN-Cy with hydrophobic surface characteristics was only suspended in chloroform, while HMSN-CyL could be well dispersed in water. The TGA curves of various nanoparticles are revealed in Fig. 1f. For HMSN-Cy, the extra 5% weight loss compared with HMSN-SH could be due to the decomposition of Cypate. The overall weight loss of HMSN-CyL was up to 21% compared to HMSN-SH, demonstrating successful coating of the phospholipid layer. The weight percentage of the phospholipid layer was calculated as 14%. These experimental results designated that the HMSN nanoparticles owned proper particle sizes for passive targeting of tumors and could obtain

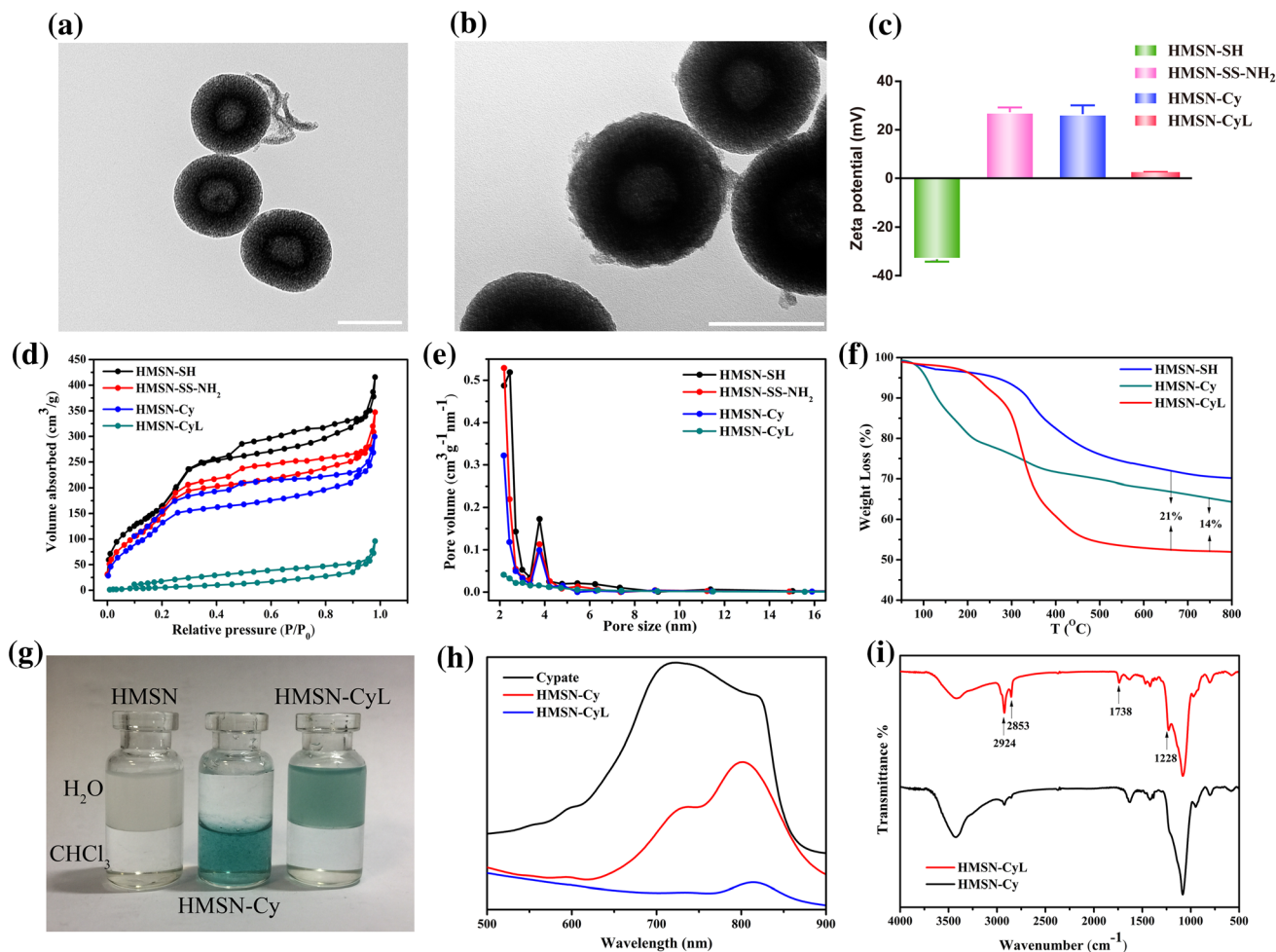


Figure 1 **a** TEM image of HMSN. **b** TEM image of HMSN-CyL. (Scale bar represents 200 μm). **c** Corresponding zeta potentials of HMSN-SH, HMSN-SS-NH₂, HMSN-Cy, HMSN-CyL. Data were presented as mean \pm SD ($n = 3$). **d** Nitrogen adsorption/desorption isotherms and **e** pore size distribution curves of

HMSN-SH, HMSN-SS-NH₂, HMSN-Cy, HMSN-CyL. **f** TGA curves of HMSN-SH, HMSN-Cy, HMSN-CyL. **g** Photograph of the distribution of HMSN, HMSN-Cy, and HMSN-CyL in water and CHCl₃. **h** Vis-NIR spectra of Cypate, HMSN-Cy, and HMSN-CyL. **i** FT-IR spectra of HMSN-Cy and HMSN-CyL.

significant drug loading capacity because of their large specific surface area.

Photothermal heating effect

Vis-NIR scanning spectra results showed that both HMSN-Cy and HMSN-CyL have strong absorption in the NIR short-wavelength band (Fig. 1h), revealing their potential NIR photothermal conversion capability. With the intention of explore the NIR photothermal properties of HMSN-CyL, temperature rise curve of HMSN-CyL aqueous dispersion was first studied. As shown in Fig. 2a, b, there was no significant temperature change in the water and blank HMSN groups. Simultaneously, when the concentration was increased from 50 $\mu\text{g}/\text{mL}$ to 500 $\mu\text{g}/\text{mL}$,

the temperature of HMSN-CyL suspension increased rapidly, indicating that HMSN-CyL carrier has a concentration-dependent photothermal conversion characteristic. Similarly, HMSN-CyL with a uniform concentration of 500 $\mu\text{g}/\text{mL}$ was exposed to a series of power density gradients (0.25–2.0 W/cm^2) for 3 min, and the temperature gradually increased with the increasing power densities. Photographs of distilled water and HMSN-CyL suspension with or without NIR irradiation are shown in Fig. 2c. After 3 min of irradiation at 2 W/cm^2 , the temperature of HMSN-CyL increased to 63.1 $^{\circ}\text{C}$, and other samples exposed to different powers had different degrees of temperature rise. After 3 min of irradiation (0.5 W/cm^2), the temperature of the suspension rose by

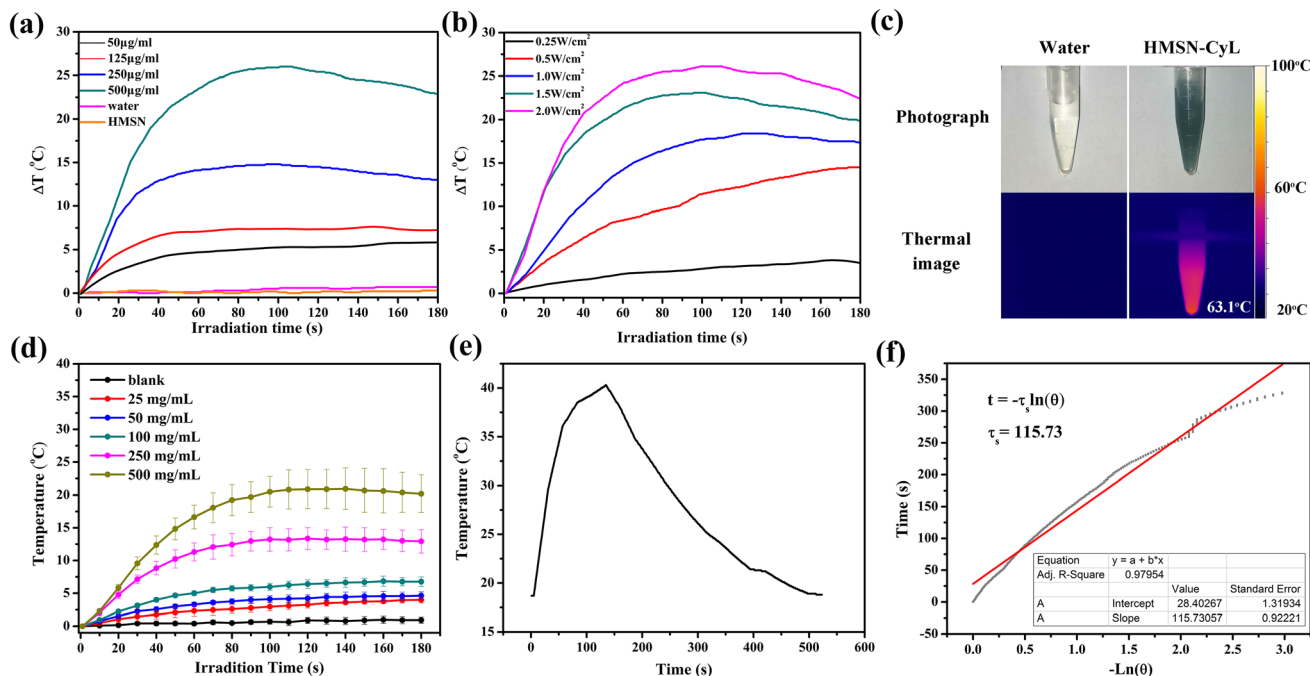


Figure 2 **a** Photothermal heating profiles of HMSN-CyL suspensions with series of concentrations varying from 50 to 500 $\mu\text{g/mL}$. **b** Photothermal heating profiles of HMSN-CyL suspensions (500 $\mu\text{g/mL}$) under series of power intensities varying from 0.25 to 2 W/cm^2 . **c** Photograph of distilled water and HMSN-CyL suspensions and thermal images of distilled water and HMSN-CyL suspensions under NIR irradiation at 2 W/cm^2

14.5 $^{\circ}\text{C}$, which had already exceeded the heat tolerance temperature of the tumor demonstrating the killing ability against tumor cells. Further, the photothermal conversion efficiency (η) was calculated to be 14.1% according to the obtained data (Fig. 2e, f). The good efficiency of the photothermal conversion supported HMSN-CyL as a promising PTT carrier.

As expected, these results indicated that HMSN-CyL had excellent photothermal conversion capability. The cellular photothermal effect of HMSN-CyL is shown in Fig. 2d. There was no noteworthy change in the temperature of the blank cell group, representing that the cells themselves do not have a photothermal effect. In contrast to the blank group, HMSN-CyL, which was increased in concentration from 20 to 500 $\mu\text{g/mL}$, was incubated with the cells, and the temperature of the cell suspension increased after irradiation. The temperature of the cell suspension raised since HMSN-CyL endocytosed by 4T1 cells converted the NIR laser power into heat. As with the in vitro results, the photothermal effect of the cells was significantly enhanced as the concentration of

for 3 min. **d** Photothermal heating profiles of 4T1 cells pretreatment with different concentrations of HMSN-CyL at 1.5 W/cm^2 . Data were presented as mean \pm SD ($n = 3$). **e** Photothermal effect of an aqueous dispersion of HMSN-CyL (500 $\mu\text{g/mL}$) under NIR laser irradiation (2 W/cm^2). **f** Linear time data versus $-\ln\theta$ obtained from the cooling stage of e.

HMSN-CyL increased. As with the in vitro results, the photothermal effect of the cells increased significantly. All the experimental results above signposted that HMSN-CyL could be an encouraging candidate for PTT.

Drug loading capacity and drug existing state in drug delivery system

The drug leakage during the modification process should be avoided in the preparation of the “gated” HMSN. In this case, HMSN-Cy was used as a carrier for drug loading process. Aiming to study the drug loading and drug release properties of nanoparticles, the anticancer drug DOX was selected as a model drug. Since the pore volume and size of HMSN-Cy were largely retained, DOX could be simply loaded into the pore by physical adsorption. Since HMSN-Cy was hydrophobic and well dispersible in methanol, the drug loading process was carried out in methanol. Due to the strong adsorption between DOX and silanol of HMSN, the weight of the encapsulated

DOX cannot be directly measured. Therefore, the weight loss method was used to calculate the loading amount of DOX by subtracting the amount of the drug which was not encapsulated after the adsorption equilibrium from the initially added amount. After adsorption of the drug, the phospholipid layer was coated, in which trace amounts of DOX leaked from the pores, but the final drug loading was still up to 35.77%, and the encapsulation efficiency was 98.14% (Tab. S3).

The Vis–NIR spectra are shown in Fig. S2. For HMSN, the absorbance decreased slowly with increasing wavelength in the visible and NIR regions. Free DOX had a maximum absorption peak around 482 nm. After DOX was loaded into HMSN, the maximum absorption peaks of DOX/HMSN and DOX/HMSN-CyL showed red shift slightly compared to free DOX. In addition, after Cypate was modified on the surface of HMSN, an absorption peak around 820 nm attributed to the grafted Cypate in DOX/HMSN-CyL was observed, which proved that the system had been successfully synthesized. The existing state of DOX in the nanocarriers was then measured by XRD and DSC. It can be seen from Fig. 3a, b that the sharp diffraction peaks and the melting point endothermic peaks of drug appeared in the physical mixture and raw DOX. Both peaks disappeared significantly after DOX was loaded into the nanoparticles presenting that DOX was loaded in the mesoporous channel in an amorphous state owing to the restriction of the mesoporous shell of HMSN [36].

Multi-stimuli triggered drug release

From the nitrogen adsorption–desorption measurement experiment results, it was known that by co-assembly of HMSN-Cy with phospholipid layer, most of the mesopores in HMSN were covered. Further, drugs were expected to be specifically released in the tumor region, so disulfide bonds were inserted between HMSN and Cypate considering the high redox environment of tumor cells. After HMSN-CyL was internalized by tumor cells, disulfide bonds would be broken by highly concentrated GSH, leading to disintegration of Cypate and phospholipid layer. It is well known that the pH values in the early endosomes and late endosomes/lysosomes of cancer cells are approximately 5.5 and 5.0, respectively. The tumor microenvironment was more acidic than the humoral environment, and the cytoplasmic GSH

levels were also orders of magnitude higher than normal tissue. These characteristics lay the foundation for the construction of pH/redox responsive systems. The release profiles of DOX/HMSN-CyL under different environments are shown in Fig. 3d. Without GSH, the cumulative release of DOX from DOX/HMSN-CyL was very slow, only 10% and 16% in pH 7.4 PBS and pH 5.0 PBS within 24 h, demonstrating that the dense layer formed by Cypate and phospholipids could block the channels and reduce DOX pre-leakage during cycling. In pH 7.4 PBS, the DOX release rate was much slower than pH 5.0 PBS. This was due to that the electrostatic interaction between DOX and the silanol groups of HMSN in pH 7.4 PBS is stronger than the electrostatic interaction in pH 5.0 PBS [37, 38]. Unsurprisingly, the accelerated release of DOX could be detected in the presence of GSH owing to the removal of Cypate and phospholipid layer. 38% of the DOX payload in DOX/HMSN-CyL was released in pH 5.0 PBS with 10 mM GSH which was almost twice that of the group without GSH. Likewise, the same trend was also observed under pH 7.4 PBS. The cleavage of disulfide bonds was investigated by studying the TGA curve of the nanocarrier after shaking for 12 h under different concentrations of GSH solution. As the concentration of GSH decreased, weight loss increased significantly (Fig. 3c), which showed that disulfide bonds broke more easily at high GSH concentration, leading to lay the foundation for the rapid release of DOX.

To check whether the NIR photothermal effect produced by Cypate could also trigger the accelerated release of DOX, the release curves under NIR light irradiation were investigated. As shown in Fig. 3e, f, DOX showed accelerated release characteristics after each irradiation, proving that the PTT effect produced by Cypate under NIR irradiation could promote DOX release [17, 39, 40]. The reasons for this spectacle were that the high temperature generated by Cypate accelerated the molecular motion, weakened the electrostatic interaction between the silanol groups of HMSN and the DOX, and reduced the density of the hydrophobic layer, thus leading to speedy diffusion of drugs. The highest percent release of DOX was observed for the NIR plus GSH group, revealing that the combination of GSH and PTT further accelerated the disintegration of the barrier layer. Since HMSN-CyL had redox/NIR dual-response characteristics, specific drug release at the tumor site could be achieved.

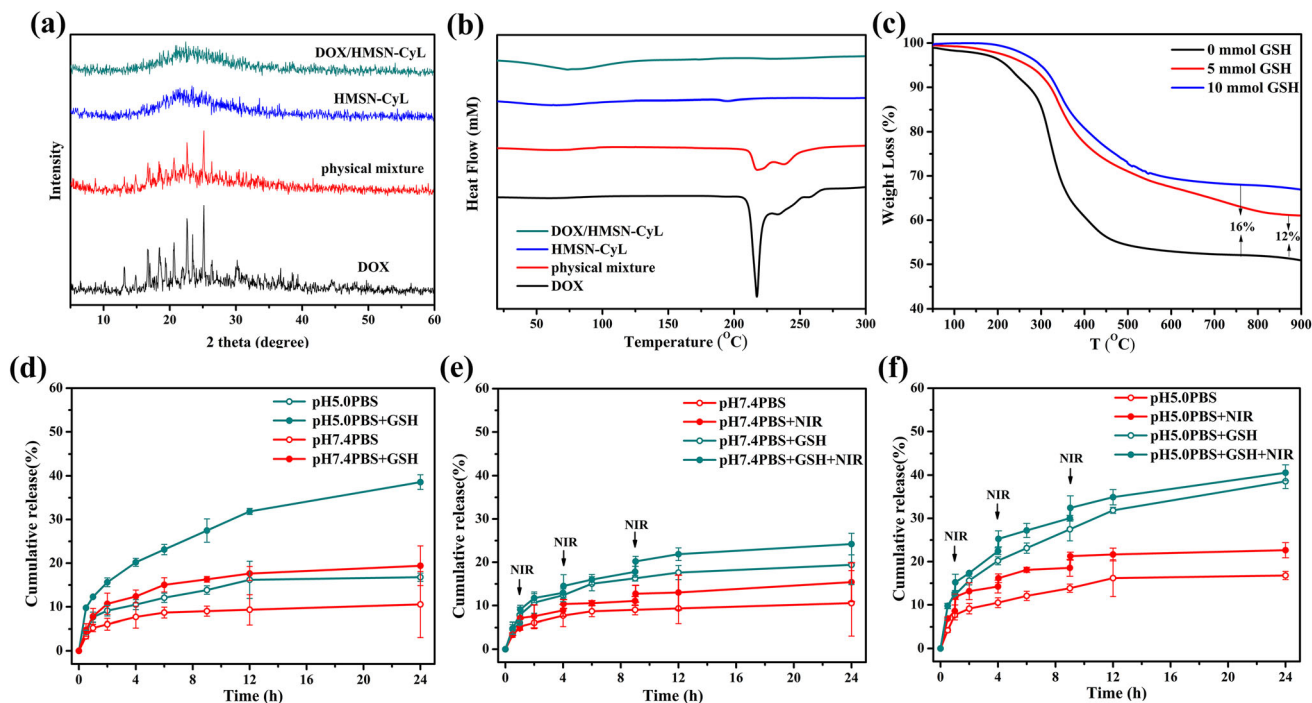


Figure 3 **a** XRD and DSC. **b** Pattern of DOX, HMSN-CyL, DOX/HMSN-CyL, and the physical mixture of DOX and HMSN-CyL. **c** TGA curves of HMSN-CyL in different amounts of GSH. Release profiles of DOX/HMSN-CyL with or without NIR

irradiation for 2 min at the power density of 1.5 W/cm^2 in **d** pH 7.4 PBS and **e** pH 5.0 PBS ($n = 3$). **f** Release profiles of DOX from DOX/HMSN-CyL at different pH values with or without 10 mM GSH. Data were presented as mean \pm SD ($n = 3$).

Dispersion stability, hemocompatibility validation, and BSA adsorption

Although HMSN is a promising drug delivery material, its clinical applications could be limited by its aggregation, hemolytic properties, and non-specific binding in the blood [41]. HMSN tends to aggregate in physiological saline and accelerates aggregation after binding to proteins in serum, resulting in rapid clearance by the reticuloendothelial system (RES) [42], which is highly undesirable. The amounts of BSA adsorbed on the surface of HMSN nanoparticles were quantified as shown in Fig. 4c. For HMSN-SH, the adsorbed BSA amount was calculated to be 25.20%. After phospholipid modification, the adsorbed BSA amount was significantly reduced to 4.54% attributing to the steric hindrance provided by PEG-modified phospholipid layer.

The sedimentation phenomenon of nanoparticles is another problem that cannot be ignored. Although HMSN-SH and HMSN-CyL were both stable in deionized water, flocculation still occurred within 24 h after dispersion of HMSN-SH in pH 7.4 PBS (Fig. 4a). However, HMSN-CyL showed good

dispersibility and could keep stable in pH 7.4 PBS for one day without precipitation. Figure 4b shows that the hydrodynamic diameter and PDI of HMSN-CyL nanoparticles were relatively constant in the aqueous dispersion medium and pH 7.4 PBS. With the extension of the standing time (24 h), the particle size of HMSN-CyL in water was 228.4 nm with a PDI of 0.22, and the particle size in pH 7.4 PBS was 271.2 nm with a PDI of 0.15. HMSN-CyL did not significantly sedimentation owing to the shielding effect of the neutrally charged phospholipid layer and PEG chains in DSPE-PEG₂₀₀₀. The steric hindrance between hydrophilic PEG-grafted nanoparticles allowed them to keep stable in PBS (pH 7.4), while the PEG chain could help avoiding the recognition and capture of RES and also prolong cycle times to promote EPR effects in tumors. In addition, hemocompatibility of HMSN-CyL nanoparticles was also investigated to assess their safety to blood cells. As shown in Fig. 4d, compared with HMSN-SH, no obvious hemolysis spectacle was seen in HMSN-CyL after 4 h still standing. At the HMSN-CyL of 1000 $\mu\text{g/mL}$, the hemolysis rate was still less than 1%, and it was more credible to see through Fig. 4e. Silica-induced

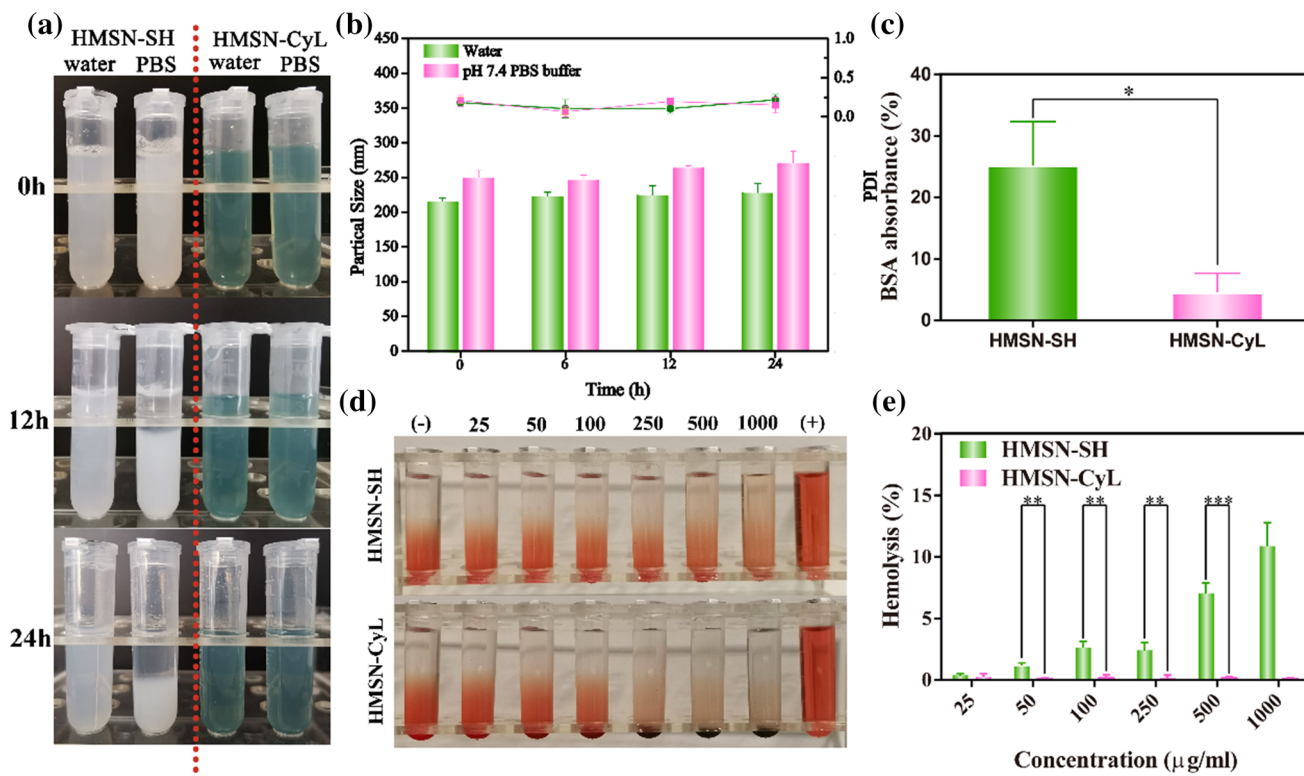


Figure 4 a Images of HMSN-SH and HMSN-CyL dispersed in water and pH 7.4 PBS. b Particle sizes and PDIs of HMSN-CyL dispersed in water and PBS (pH 7.4), respectively, at different standing times (0, 6, 12, 24 h). c BSA absorbance of HMSN-SH

and HMSN-CyL. d Hemolytic photographs and e hemolysis percentage of HMSN-SH and HMSN-CyL at different concentrations ($\mu\text{g}/\text{mL}$). Data were presented as mean \pm SD ($n = 3$, $*p < 0.05$, $**p < 0.01$, $***p < 0.001$).

hemolysis was attributed to that silica had a high attraction to bind to the abundant tetra-alkylammonium groups on the RBC membrane, and this property could subsequently lead to the production of reactive oxygen species (ROS) and denaturation of membrane proteins after intimate contact with silicates [43, 44]. Nevertheless, after being shielded by the phospholipid layer, HMSN-Cy had a significant improvement in experimental results of protein adsorption, hemolysis, or nanoparticle aggregation. All of the above results demonstrated that HMSN-CyL was non-toxic and safe enough for drug delivery.

Photothermal therapy effect on cytological level

To investigate the photothermal effect of Cypate at the cellular level, 4T1 cells were co-cultured with different concentrations of HMSN-CyL and irradiated for the same time at different light intensities. It is well known that PI can enter dead or apoptotic

cells and bind to DNA in the nuclear to produce intense red fluorescence, while Calcein-AM can be hydrolyzed by endogenous esterases in the cytoplasm of living cells to produce green fluorescence. 4T1 cells were irradiated with gradient power densities of 808 nm laser after incubation with 250 $\mu\text{g}/\text{mL}$ of HMSN-CyL nanoparticles (Fig. 5a). It was apparent that the same phenomenon could be observed in the group without NIR irradiation and the control group, demonstrating that HMSN-CyL had negligible cytotoxicity. After cells were incubated with 250 $\mu\text{g}/\text{mL}$ carrier, the red fluorescence signal in cells gradually increased with the increasing power densities of irradiation, and the green fluorescence signal gradually decreased, signifying that cells experienced significant apoptosis after irradiation, and the photothermal effect was power dependent to some extent. To further demonstrate that the PTT effect was concentration dependent, 4T1 cells were cultured with 500 $\mu\text{g}/\text{mL}$ HMSN-CyL and illuminated at 2 W/cm^2 (Fig. 5b). Compared to the 250 $\mu\text{g}/\text{mL}$ HMSN-CyL, a more intense red light and

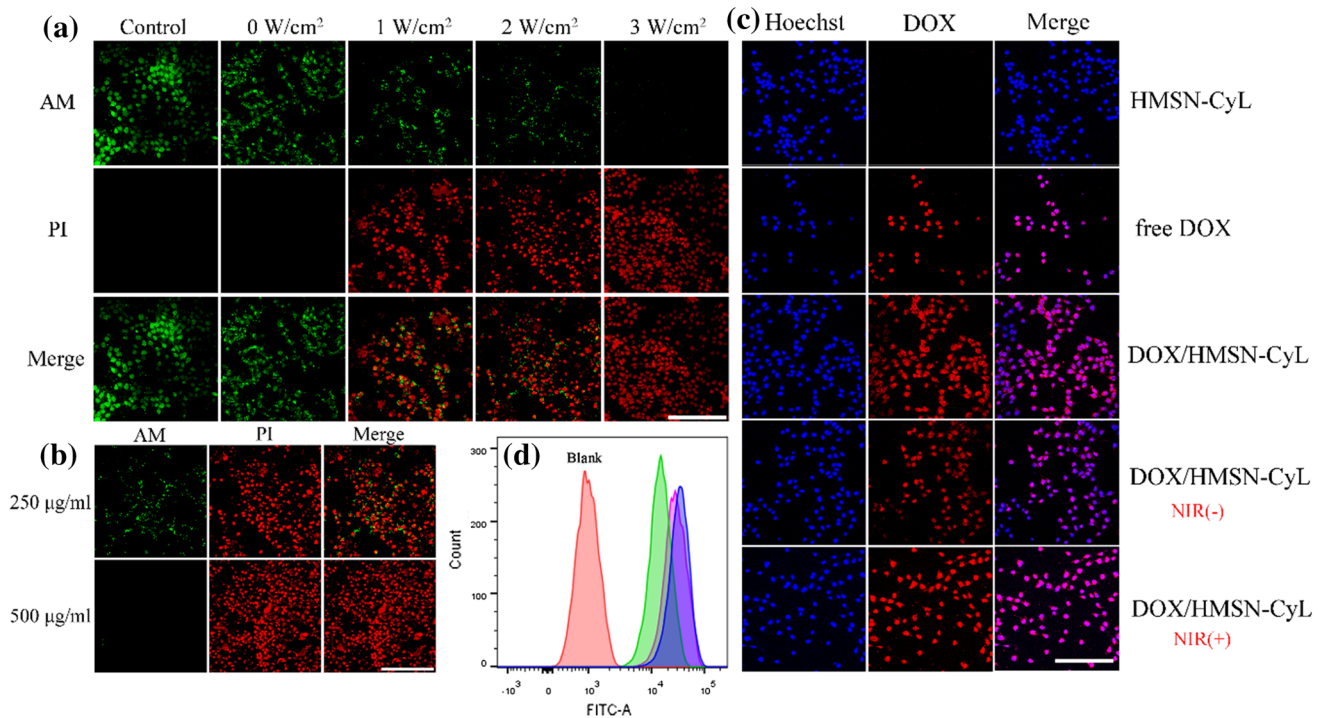


Figure 5 **a** Fluorescence images of 4T1 cells incubated with HMSN-CyL after laser irradiation under different powers and co-stained with Calcein-AM (live cells, green) and PI (dead cells, red). **b** Fluorescence pictures of 4T1 cells treated with different densities of HMSN-CyL under NIR irradiation (2 W/cm²). Cellular uptake: **c** CLSM images of 4T1 cells incubated with

free DOX and DOX/HMSN-CyL with NIR irradiation or not for 2 h. **d** FCM analysis of 4T1 cells incubated with different suspensions (green stands for DOX group, pink stands for DOX/HMSN-CyL group, and blue stands for DOX/HMSN-CyL with NIR group, scale bar represents 200 µm).

almost negligible green light were detected in this group, representing that almost all the cells died. The conceivable reasons were the photothermal effect greatly increased the permeability of the cell membrane and the cell endogenous esterases were inactivated. The above experimental results confirmed that HMSN-CyL had good biocompatibility and superior photothermal potential.

Cell uptake and bioimaging

Adequate cellular internalization of DOX/HMSN-CyL was particularly beneficial for effective chemotherapy and photothermal combination therapy in tumor cells. Herein, CLSM and FCM were employed to investigate the cell uptake of DOX/HMSN-CyL (Fig. 5c, d). HMSN-CyL could be used as a control, and it only exhibited blue fluorescence under the microscope. In addition, after cells was incubated with DOX, red fluorescence was observed due to the fluorescent property of DOX itself. The red and blue fluorescence signals overlapped each other,

demonstrating that the DOX had diffused into the nucleus. Significant red fluorescence appeared in the cytoplasm after 4T1 cells were incubated with DOX/HMSN-CyL, indicating that after DOX/HMSN-CyL had been taken up by cells, DOX gradually released into the cytoplasm and diffused into the nucleus. To study the effect of irradiation, fresh medium was used instead of the medicated medium. The experimental results are shown in Fig. 5c. Under NIR irradiation, the red fluorescence of DOX from DOX/HMSN-CyL was more obvious than in the group without NIR irradiation, which proved that the PTT effect produced by laser irradiation could promote the release of DOX from DOX/HMSN-CyL. However, the DOX/HMSN-CyL group without NIR irradiation had a weaker DOX fluorescence intensity than the DOX/HMSN-CyL group because the DOX concentration in the fresh medium was lower than the concentration in the cells, causing escapement of DOX from the cells. The results indicated that DOX/HMSN-CyL could be internalized by 4T1 cells and the heat generated by NIR irradiation could

accelerate drug release inside the cells by increasing the thermal movement of molecules [45]. The FCM assay quantitatively assessed the cell uptake of DOX/HMSN-CyL by measuring DOX fluorescence in cells as well. As shown in Fig. 5d, the fluorescence intensity of DOX increased due to the irradiation of NIR light, which showed that the high temperature generated by PTT could promote the release of DOX. The fluorescence intensity increased of DOX due to the irradiation of NIR light, demonstrating an increase in DOX/HMSN-CyL cell internalization. The quantitative analysis of the mean fluorescence intensity results is shown in Fig. S3, indicating that the level of endocytosis of DOX/HMSN-CyL by 4T1 cells was

significantly increased after NIR laser irradiation ($p < 0.001$), much higher than that of free DOX, which was consistent with CLSM results.

In vitro cytotoxicity testing

Cytotoxicity experiments and MCTs experiments were designed to evaluate the in vitro biocompatibility and antitumor ability of prepared nanoparticles using 4T1 cells. The cytotoxicity test results are revealed in Fig. 6b, c. The cell viability of HMSN-CyL was more than 80% without NIR irradiation, indicating that HMSN-CyL had negligible toxicity and safety. As for NIR irradiation group, the cell viability

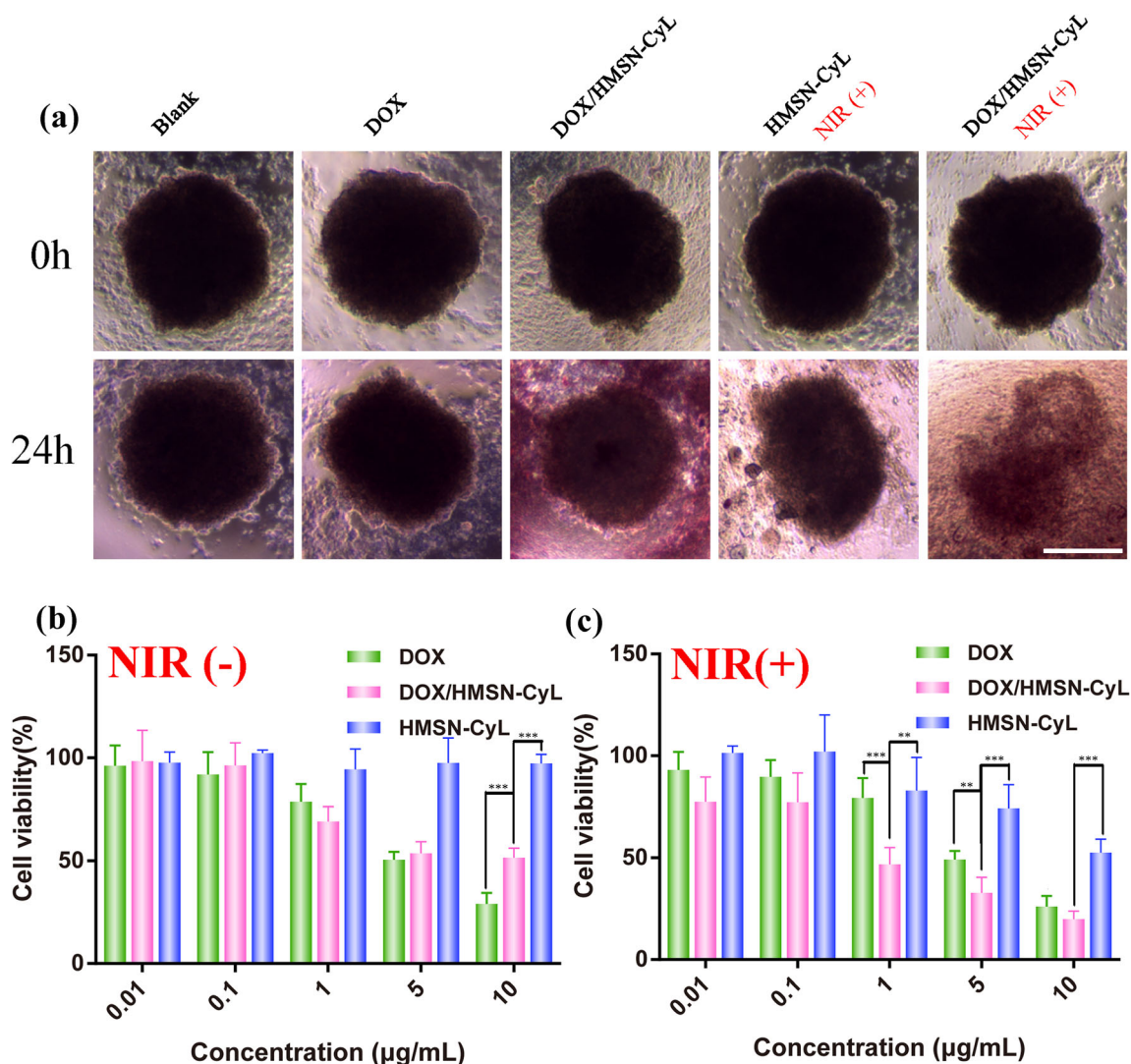


Figure 6 a Optical images of 4T1 tumor spheres treated with different preparations at 0 h and 24 h. The cell viabilities of 4T1 cells incubated with various concentrations of free DOX, DOX/

HMSN-CyL, and HMSN-CyL c with or b without NIR laser irradiation. Data were presented as mean \pm SD ($n = 3$, $*p < 0.05$, $**p < 0.01$, $***p < 0.001$).

and concentration of HMSN-CyL were negatively dependent, indicating that the heat generated by NIR irradiation can cause tumor cell death. It is well known that cells and tissues have no apoptosis or necrosis under NIR irradiation, and there is no therapeutic effect on tumors only with NIR irradiation [46], proving that NIR laser is safe and feasible for normal biology [47, 48], which is consistent with MTT results. For free DOX group, cell viability was negatively correlated with the increase in DOX concentration regardless of whether NIR was used, and there was no momentous difference between two groups, indicating that NIR had no significant cytotoxicity to cells. As expected, compared with just PTT or chemotherapy, 4T1 cells treated with the DOX/HMSN-CyL nanoparticles with NIR irradiation had the lowest cell viability, showing a marked chemo-photothermal combination therapeutic effect. Additionally, the IC_{50} value is exhibited in Table 1. For the free DOX group, there was no significant difference in IC_{50} values under NIR irradiation or not, also indicating that NIR had no significant cytotoxicity to cells. However, IC_{50} values decreased from 7.49 $\mu\text{g}/\text{mL}$ (without NIR) to 0.66 $\mu\text{g}/\text{mL}$ (with NIR) in DOX/HMSN-CyL group, indicating that DOX/HMSN-CyL had the best effect under NIR irradiation and could quickly kill tumor cell. Besides, CI was calculated to be 0.26, demonstrating that the combination chemotherapy and PTT could have an markedly synergistic effect in tumor diseases [49]. This may be attributed to that the high temperature could not only destroy tumor cells, but also increase the cell sensitivity to chemotherapeutic drugs, thus resulting in a maximum cytotoxicity. DOX/HMSN-CyL could be used as a promising carrier for PTT and chemotherapy combination therapy.

To further investigate the effective lethality of DOX/HMSN-CyL on tumors of breast cancer, MCTs model was established to mimic actual tumors (Fig. 6a). Compared with the control group, the MCTs of each treatment group showed some degree of collapse and

Table 1 IC_{50} values of HMSN-CyL, free DOX, and DOX/HMSN-CyL samples with/without NIR irradiation against 4T1 cells

| Preparations | IC_{50} ($\mu\text{g}/\text{mL}$) | |
|--------------|---------------------------------------|------|
| | Without NIR | NIR |
| HMSN-CyL | – | 16.1 |
| DOX | 4.25 | 3.79 |
| DOX/HMSN-CyL | 7.49 | 0.66 |

separation, especially in the combination treatment group that DOX/HMSN-CyL had the best therapeutic effect with NIR irradiation which was consistent with the results of cytotoxicity experiments mentioned above. Both the cell experiments had demonstrated the chemotherapy and hyperthermia synergistic treatment. So far, these exciting findings have proved the cytotoxic function features of the DOX/HMSN-CyL, and the combination of chemotherapy and hyperthermia provides a new attempt and meaningful exploration for the treatment of tumors.

Conclusion

This paper designed a novel antitumor drug delivery nanoplatfrom mediated by hydrophobic interactions for the combined treatment of cancer. The good photothermal conversion agent Cypate was bonded to the surface of HMSN by cleavable disulfide bonds, and then, DPPC and DSPE-PEG₂₀₀₀ were further coated on the surface of HMSN-Cy through hydrophobic interactions. For the first time, HMSN and Cypate were combined, followed by DOX loading to produce a chemo-photothermal combination therapy. In conclusion, DOX/HMSN-CyL was an excellent antitumor drug delivery nanoplatfrom with many advantages: (1) DOX, in an amorphous form, was loaded in DOX/HMSN-CyL with a high loading amount of 35.77%; (2) The system had a pH/GSH/NIR multi-stimuli-responsive characteristic, which could accurately carry out drug delivery and controlled release at the tumor site; (3) The composite phospholipid-coated carrier improved the biocompatibility and dispersion stability under physiological conditions and prevented the premature release of DOX; (4) cytotoxicity tests showed that DOX/HMSN-CyL displayed synergy through a combination of PTT and chemotherapy, with a CI of 0.26. MCTs experiments were also performed, and the treatment effect of the combination treatment group remained the best. The results of all experiments indicate that this study offers great potentials in the multi-trigger drug delivery as well as combination therapy.

Acknowledgements

This work was supported by National Natural Science Foundation of China (Nos. 81603058 and

81473165) and Career Development Program for Young Teachers in Shenyang Pharmaceutical University (No. ZQN2016025).

Compliance with ethical standards

Conflict of interest The authors declare that they have no conflict of interest.

Electronic supplementary material: The online version of this article (<https://doi.org/10.1007/s10853-019-04314-w>) contains supplementary material, which is available to authorized users.

References

- [1] Chen W, Zhong P, Meng F, Cheng R, Deng C, Feijen J et al (2013) Redox and pH-responsive degradable micelles for dually activated intracellular anticancer drug release. *J Control Release* 169:171–179
- [2] Kim T-W, Slowing II, Chung P-W, Lin VS-Y (2010) Ordered Mesoporous polymer–silica hybrid nanoparticles as vehicles for the intracellular controlled release of macromolecules. *ACS Nano* 5:360–366
- [3] Lee CH, Cheng SH, Huang IP, Souris JS, Yang CS, Mou CY et al (2010) Intracellular pH-responsive mesoporous silica nanoparticles for the controlled release of anticancer chemotherapeutics. *Angew Chem Int Ed* 49:8214–8219
- [4] Cheng R, Feng F, Meng F, Deng C, Feijen J, Zhong Z (2011) Glutathione-responsive nano-vehicles as a promising platform for targeted intracellular drug and gene delivery. *J Control Release* 152:2–12
- [5] Cui Y, Dong H, Cai X, Wang D, Li Y (2012) Mesoporous silica nanoparticles capped with disulfide-linked PEG gatekeepers for glutathione-mediated controlled release. *ACS Appl Mater Interfaces* 4:3177–3183
- [6] Wang J, Sun X, Mao W, Sun W, Tang J, Sui M et al (2013) Tumor redox heterogeneity-responsive prodrug nanocapsules for cancer chemotherapy. *Adv Mater* 25:3670–3676
- [7] Luo C, Sun J, Liu D, Sun B, Miao L, Musetti S et al (2016) Self-assembled redox dual-responsive prodrug-nanosystem formed by single thioether-bridged paclitaxel-fatty acid conjugate for cancer chemotherapy. *Nano Lett* 16:5401–5408
- [8] Zou Z, He X, He D, Wang K, Qing Z, Yang X et al (2015) Programmed packaging of mesoporous silica nanocarriers for matrix metalloprotease 2-triggered tumor targeting and release. *Biomaterials* 58:35–45
- [9] Liang L, Lin S-W, Dai W, Lu J-K, Yang T-Y, Xiang Y et al (2012) Novel cathepsin B-sensitive paclitaxel conjugate: Higher water solubility, better efficacy and lower toxicity. *J Control Release* 160:618–629
- [10] Lu J, Choi E, Tamanoi F, Zink JI (2008) Light-activated nanoimpeller-controlled drug release in cancer cells. *Small* 4:421–426
- [11] Yang G, Sun X, Liu J, Feng L, Liu Z (2016) Light-responsive, singlet-oxygen-triggered on-demand drug release from photosensitizer-doped mesoporous silica nanorods for cancer combination therapy. *Adv Funct Mater* 26:4722–4732
- [12] Xiao W, Chen WH, Xu XD, Li C, Zhang J, Zhuo RX et al (2011) Design of a cellular-uptake-shielding “plug and play” template for photo controllable drug release. *Adv Mater* 23:3526–3530
- [13] Fang W, Tang S, Liu P, Fang X, Gong J, Zheng N (2012) Pd nanosheet-covered hollow mesoporous silica nanoparticles as a platform for the chemo-photothermal treatment of cancer cells. *Small* 8:3816–3822
- [14] Liu Y, Ai K, Liu J, Deng M, He Y, Lu L (2013) Dopamine-melanin colloidal nanospheres: an efficient near-infrared photothermal therapeutic agent for in vivo cancer therapy. *Adv Mater* 25:1353–1359
- [15] Lee S-M, Kim HJ, Kim SY, Kwon M-K, Kim S, Cho A et al (2014) Drug-loaded gold plasmonic nanoparticles for treatment of multidrug resistance in cancer. *Biomaterials* 35:2272–2282
- [16] Pan Y, Le Z, Zeng L, Ren W, Xiao X, Zhang J et al (2016) Gd-based upconversion nanocarriers with yolk–shell structure for dual-modal imaging and enhanced chemotherapy to overcome multidrug resistance in breast cancer. *Nanoscale* 8:878–888
- [17] Xing Y, Zhang J, Chen F, Liu J, Cai K (2017) Mesoporous polydopamine nanoparticles with co-delivery function for overcoming multidrug resistance via synergistic chemo-photothermal therapy. *Nanoscale* 9:8781–8790
- [18] Li Y, Xu X, Zhang X, Li Y, Zhang Z, Gu Z (2016) Tumor-specific multiple stimuli-activated dendrimeric nanoassemblies with metabolic blockade surmount chemotherapy resistance. *ACS Nano* 11:416–429
- [19] Zhang Z, Wang J, Chen C (2013) Near-infrared light-mediated nanoplatforms for cancer thermo-chemotherapy and optical imaging. *Adv Mater* 25:3869–3880
- [20] Deng Y, Käfer F, Chen T, Jin Q, Ji J, Agarwal S (2018) Let there be light: polymeric micelles with upper critical solution temperature as light-triggered heat nanogenerators for combating drug-resistant cancer. *Small* 14:1802420
- [21] Yu H, Cui Z, Yu P, Guo C, Feng B, Jiang T et al (2015) pH- and NIR light-responsive micelles with hyperthermia-triggered tumor penetration and cytoplasm drug release to reverse doxorubicin resistance in breast cancer. *Adv Funct Mater* 25:2489–2500

- [22] Liu Q, Guo B, Rao Z, Zhang B, Gong JR (2013) Strong two-photon-induced fluorescence from photostable, biocompatible nitrogen-doped graphene quantum dots for cellular and deep-tissue imaging. *Nano Lett* 13:2436–2441
- [23] Wu X, Ming T, Wang X, Wang P, Wang J, Chen J (2009) High-photoluminescence-yield gold nanocubes: for cell imaging and photothermal therapy. *ACS Nano* 4:113–120
- [24] Yang K, Zhang S, Zhang G, Sun X, Lee S-T, Liu Z (2010) Graphene in mice: ultrahigh in vivo tumor uptake and efficient photothermal therapy. *Nano Lett* 10:3318–3323
- [25] Su S, Ding Y, Li Y, Wu Y, Nie G (2016) Integration of photothermal therapy and synergistic chemotherapy by a porphyrin self-assembled micelle confers chemosensitivity in triple-negative breast cancer. *Biomaterials* 80:169–178
- [26] Deng Y, Huang L, Yang H, Ke H, He H, Guo Z et al (2017) Cyanine-Anchored Silica Nanochannels for Light-Driven Synergistic Thermo-Chemotherapy. *Small* 13:1602747
- [27] Wang L, Kim M, Fang Q, Min J, Jeon WI, Lee SY et al (2013) Hydrophobic end-gated silica nanotubes for intracellular glutathione-stimulated drug delivery in drug-resistant cancer cells. *Chem Commun* 49:3194–3196
- [28] Treger JS, Priest MF, Iezzi R, Bezanilla F (2014) Real-time imaging of electrical signals with an infrared FDA-approved dye. *Biophys J* 107:L09–L12
- [29] Fu C, Liu T, Li L, Liu H, Chen D, Tang F (2013) The absorption, distribution, excretion and toxicity of mesoporous silica nanoparticles in mice following different exposure routes. *Biomaterials* 34:2565–2575
- [30] Liu T, Li L, Teng X, Huang X, Liu H, Chen D et al (2011) Single and repeated dose toxicity of mesoporous hollow silica nanoparticles in intravenously exposed mice. *Biomaterials* 32:1657–1668
- [31] Ye Y, Li WP, Anderson CJ, Kao J, Nikiforovich GV, Achilefu S (2003) Synthesis and characterization of a macrocyclic near-infrared optical scaffold. *J Am Chem Soc* 125:7766–7767
- [32] Fang X, Chen C, Liu Z, Liu P, Zheng N (2011) A cationic surfactant assisted selective etching strategy to hollow mesoporous silica spheres. *Nanoscale* 3:1632–1639
- [33] Zhao Q, Liu J, Zhu W, Sun C, Di D, Zhang Y et al (2015) Dual-stimuli responsive hyaluronic acid-conjugated mesoporous silica for targeted delivery to CD44-overexpressing cancer cells. *Acta Biomater* 23:147–156
- [34] Ebright YW, Chen Y, Kim Y, Ebright RH (1996) S-[2-(4-Azidosalicylamido) ethylthio]-2-thiopyridine: radioiodinatable, cleavable, photoactivatable cross-linking agent. *Bioconjugate Chem* 7:380–384
- [35] Jiao J, Li X, Zhang S, Liu J, Di D, Zhang Y et al (2016) Redox and pH dual-responsive PEG and chitosan-conjugated hollow mesoporous silica for controlled drug release. *Mater Sci Eng C* 67:26–33
- [36] Tina U, Aljaz G, Odon PE, Venčeslav KI, Gregor M, Miran GE (2011) The phase (trans)formation and physical state of a model drug in mesoscopic confinement. *Phys Chem Chem Phys* 13:16046–16054
- [37] Tang H, Guo J, Sun Y, Chang B, Ren Q, Yang W (2011) Facile synthesis of pH sensitive polymer-coated mesoporous silica nanoparticles and their application in drug delivery. *Int J Pharm* 421:388–396
- [38] Yufang Z, Toshiyuki I, Nobutaka H, Stefan K (2010) Rattle-type $\text{Fe}_3\text{O}_4@SiO_2$ hollow mesoporous spheres as carriers for drug delivery. *Small* 6:471–478
- [39] Shen S, Tang H, Zhang X, Ren J, Pang Z, Wang D et al (2013) Targeting mesoporous silica-encapsulated gold nanorods for chemo-photothermal therapy with near-infrared radiation. *Biomaterials* 34(12):3150–3158
- [40] Zhou L, Jing Y, Liu Y, Liu Z, Gao D, Chen H et al (2018) Mesoporous carbon nanospheres as a multifunctional carrier for cancer theranostics. *Theranostics* 8(3):663
- [41] Wang LS, Wu LC, Lu SY, Chang LL, Teng IT, Yang CM et al (2010) Biofunctionalized phospholipid-capped mesoporous silica nanoshuttles for targeted drug delivery: improved water suspensibility and decreased nonspecific protein binding. *ACS Nano* 4:4371–4379
- [42] Moghimi SM, Hunter AC, Murray JC (2005) Nanomedicine: current status and future prospects. *Faseb J Off Publ Feder Am Soc Exp Biol* 19:311–330
- [43] Slowing II, Chia-Wen W, Vivero-Escoto JL, Victor S-YL (2010) Mesoporous silica nanoparticles for reducing hemolytic activity towards mammalian red blood cells. *Small* 5:57–62
- [44] Tian Y, Alexander M, Hamidreza G (2011) Impact of silica nanoparticle design on cellular toxicity and hemolytic activity. *ACS Nano* 5:5717–5728
- [45] Zhao Q, Yang Y, Wang H, Lei W, Liu Y, Wang S (2019) Gold nanoparticles modified hollow carbon system for dual-responsive release and chemo-photothermal synergistic therapy of tumor. *J Colloid Interface Sci* 554:239–249
- [46] Feng S, Mao Y, Wang X, Zhou M, Lu H, Zhao Q et al (2020) Triple stimuli-responsive ZnO quantum dots-conjugated hollow mesoporous carbon nanoplatfor for NIR-induced dual model antitumor therapy. *J Colloid Interface Sci* 559:51–64
- [47] Owens EA, Hyun H, Tawney JG, Choi HS, Henary M (2015) Correlating molecular character of NIR imaging agents with tissue-specific uptake. *J Med Chem* 58(10):4348–4356

- [48] Cheng L, Wang C, Feng L, Yang K, Liu Z (2014) Functional nanomaterials for phototherapies of cancer. *Chin J Clin Oncol* 114(21):10869–10939
- [49] Yang J, Su H, Sun W, Cai J, Liu S, Chai Y et al (2018) Dual chemodrug-loaded single-walled carbon nanohorns for multimodal imaging-guided chemo-photothermal therapy of tumors and lung metastases. *Theranostics* 8:1966–1984

Publisher's Note Springer Nature remains neutral with regard to jurisdictional claims in published maps and institutional affiliations.